Deng WQ, Li XM, Gao X *et al.* A modified fuzzy c-means algorithm for brain MR image segmentation and bias field correction. JOURNAL OF COMPUTER SCIENCE AND TECHNOLOGY 31(3): 501–511 May 2016. DOI 10.1007/s11390-016-1643-5

A Modified Fuzzy C-Means Algorithm for Brain MR Image Segmentation and Bias Field Correction

Wen-Qian Deng [1], Xue-Mei Li [1,*], Xifeng Gao [2], and Cai-Ming Zhang [1]

[1] *School of Computer Science and Technology, Shandong University, Jinan 250101, China*
[2] *Department of Computer Science, University of Houston, Houston, TX 77004, U.S.A.*

E-mail: dengwenqian@mail.sdu.edu.cn; xmli@sdu.edu.cn; gxf.xisha@gmail.com; czhang@sdu.edu.cn

Received December 2, 2015; revised March 15, 2016.

Abstract In quantitative brain image analysis, accurate brain tissue segmentation from brain magnetic resonance image (MRI) is a critical step. It is considered to be the most important and difficult issue in the field of medical image processing. The quality of MR images is influenced by partial volume effect, noise, and intensity inhomogeneity, which render the segmentation task extremely challenging. We present a novel fuzzy c-means algorithm (RCLFCM) for segmentation and bias field correction of brain MR images. We employ a new gray-difference coefficient and design a new impact factor to measure the effect of neighbor pixels, so that the robustness of anti-noise can be enhanced. Moreover, we redefine the objective function of FCM (fuzzy c-means) by adding the bias field estimation model to overcome the intensity inhomogeneity in the image and segment the brain MR images simultaneously. We also construct a new spatial function by combining pixel gray value dissimilarity with its membership, and make full use of the space information between pixels to update the membership. Compared with other state-of-the-art approaches by using similarity accuracy on synthetic MR images with different levels of noise and intensity inhomogeneity, the proposed algorithm generates the results with high accuracy and robustness to noise.

Keywords image segmentation, fuzzy c-means, bias field correction, anti-noise

1 Introduction

With the rapid development of medical imaging technology, medical image has become one of the major auxiliary means in clinical care, and greatly improved the accuracy of medical diagnosis. Current medical image segmentation technology focuses on magnetic resonance images (MRI), which has great soft tissue resolution and multi-spectral characteristics, and it is capable of multi-directional and multi-parameter imaging. Moreover, the non-radioactive imaging modalities are harmless to human beings. The advantages above make MRI quite suitable for inspecting brain lesions.

Segmentation of major brain tissues from MRI, including gray matter (GM), white matter (WM) and cerebro-spinal fluid (CSF), is a key step for both clinical diagnosis and neuroscience. Medical images are fuzzy inherently, because they are inevitably affected by random noise, magnetic field inhomogeneity and the partial volume effect caused by the limit of the imaging device resolution. These factors directly result in the fuzziness of medical images and make the segmentation process more difficult and challenging for these images.

The bias field correction for MRI has been studied extensively in the past two decades. The smoothly varying bias field, which causes the intensity of the same tissue varies with its positions, is identified as one of technical barriers in the MRI segmenta-

Regular Paper
Special Section of CVM 2016
This work was supported by the National Natural Science Foundation of China under Grant Nos. 61332015, 61373078, 61572292, and 61272430, and the National Research Foundation for the Doctoral Program of Higher Education of China under Grant No. 20110131130004.

*Corresponding Author

tion. Although this change is difficult to be observed directly, the intensity-based segmentation algorithms may produce error classification of tissues. Generally, the methods handling bias field are divided into two categories: prospective methods and retrospective methods[1]. Prospective methods[2-4] manage to avoid intensity inhomogeneity in the collection procedure by using the specific nuclear magnetic resonance (NMR) equipment. These methods can correct the bias field produced by the imaging devices and environment, but they fail to handle the inhomogeneity caused by patients. In addition, each scan needs to create a new model, which reduces the practicability of these methods in clinic. Instead, retrospective methods[5-8] are based on the image post-processing. Ignoring the source of the bias field, these methods can be applied to any MRI. Generally, these methods estimate a non-uniform multiplicative field by homomorphic filtering[9], and restore the real image by removing this field from original image.

Segmentation based method[10] is one of the most popular methods to handle the intensity inhomogeneity in retrospective methods. The bias field correction is an essential preprocessing step for medical image segmentation. In turn, the accurate segmentation makes intensity inhomogeneity correction much simpler. Thus, a method including tissues segmentation and bias field correction could handle the intensity inhomogeneity better. These bias field correction methods can be further classified according to the applied image segmentation method. The most popular one is based on the fuzzy c-means clustering algorithm (FCM)[11]. Fuzzy c-means is a soft clustering algorithm which assumes the image pixels can be classified into various categories. Due to the uncertainty of initial categories, FCM algorithm retains much more information than other segmentation methods[12], and depicts the fuzzy characteristic of medical image dramatically. Since the conventional FCM algorithm does not take any spatial information into account, it becomes very sensitive to noise and intensity inhomogeneity. Many researchers have compensated this drawback of FCM by modifying the objective function, transforming the distance measure method or incorporating the local spatial information.

Ahmed *et al.*[13] modified the objective function and proposed FCM_S algorithm. They considered that the labelling of a pixel is affected by the labels in its neighborhood. This method removes noisy spots effectively in MRI segmentation, but it is time-consuming because of taking more time to compute the labels of the neighbor pixels for each iteration[14]. Chen and Zhang[15] proposed two variants (FCM_S1 and FCM_S2) where the neighborhood terms are replaced by the mean-filter and the median-filter image respectively. Both of the methods reduce the time complexity. Chuang *et al.*[16] proposed an algorithm (SFCMpq) where the membership function is incorporated with spatial information, and makes the image region more homogeneous and less sensitive to noise. Szilagyi *et al.*[17] proposed an enhanced FCM method (EnFCM) based on gray level histogram. It calculates the linearly-weighted sum from the original image and average gray level of local neighborhood, which speeds up the computation successfully. Cai *et al.*[18] proposed a fast framework for image segmentation (FGFCM) which combines the gray and the local spatial information. Krinidis and Chatzis[19] introduced a new fuzzy factor to incorporate the local spatial factor and the gray information, and proposed FLICM algorithm which can overcome the drawbacks of conventional algorithm. Furthermore, it is able to control the trade-off between smoothing and clustering by adjusting adaptive parameters. More recently, Gong *et al.*[20] proposed an improved FLICM algorithm (KWFLICM). The algorithm is used to design a new fuzzy factor which measures the effect of neighborhood more accurately. Moreover, it uses the Gaussian kernel distance instead of the Euclidean distance, and the quality of the segmentation results is well enhanced particularly on the images with the salt and pepper noise. Although these improved approaches have been applied to different types of images successfully, there are still some defects on segmenting brain MRI. On one hand, a few algorithms fail to correct the intensity inhomogeneity and result in inaccurate segmentation. On the other hand, the estimation of influence between neighbor pixels and the central pixel is not precise enough, which leads to the inferior anti-noise performance.

In this paper, we propose a novel algorithm RCLFCM for bias field correction and image segmentation, which incorporates with neighborhood and spatial information of image. The new method redefines the impact factor between the central pixel and its neighbor pixels, modifies the objective function of FCM, and combines it with the bias field estimation model. In this way, we can conduct bias field correction and segmentation to MRI simultaneously. Moreover, we use a new spatial function incorporating the terms of the gray-level dissimilarity and membership, and update the membership matrix based on the new spatial func-

tion for each iteration. Compared with state-of-the-art segmentation techniques, the proposed method improves the robustness to the bias field correction and accuracy of tissues segmentation as shown by our experimental results.

The remaining part of this paper is organized as follows. Section 2 briefly describes the fuzzy c-means algorithm and the bias field formulation in images. The detailed RCLFCM model is introduced in Section 3. Experimental results and comparisons with existing methods are discussed in Section 4. Conclusions are given in Section 5.

2 Preliminary Theory

Fuzzy c-means clustering algorithm and bias field formulation are effective methods for medical image processing, and they are the main foundation of the proposed algorithm.

2.1 Fuzzy C-Means Clustering

Let $I = \{x_i, i = (1, 2, ..., N)\}$, where x_i is the i-th pixel of image I with dimension D. The standard FCM algorithm divides these pixels into K clusters by minimizing the objective function, and every cluster centroid is weighted by its corresponding membership. The membership function is $\boldsymbol{U} = \{u_{ik}\} \in \mathbb{R}^{K\times N}$, where $u_{ik} \in [0, 1]$ is pixel i belonging to cluster k and follows the constraint $\sum_{k=1}^{K} u_{ik} = 1$. The conventional objective function is defined as[14]:

$$J_{FCM} = \sum_{i=1}^{N}\sum_{k=1}^{K} u_{ik}^{m}||x_i - v_k||^2, \tag{1}$$

where $m \in (1, \infty)$ is the fuzzy weighting exponent upon the membership and $m = 2$ generally. $||x_i - v_k||^2$ is a Euclidean distance between point x_i and cluster center v_k. The requirements for minimizing (1) by calculating the membership value u_{ik} and the cluster centers v_k are as follows:

$$u_{ik} = \frac{1}{\sum_{j=1}^{K}(\frac{||x_i - v_k||}{||x_i - v_j||})^{2/(m-1)}},$$
$$v_k = \frac{\sum_{i=1}^{N} u_{ik}^{m} x_i}{\sum_{i=1}^{N} u_{ik}^{m}}.$$

The defuzzification process assigns pixel x_i to the cluster center v_k according to the highest membership principles, $v_k = \arg\{\max\{u_{ik}\}\}, k = 1, 2, ..., K$.

In order to overcome the sensitivity to noise, FLICM[19] introduces a fuzzy factor G_{ki} to control the weight between noise reduction and details reservation. The objective function is defined as follows:

$$J_{FLICM} = \sum_{i=1}^{N}\sum_{k=1}^{K}(u_{ik}^{m}||x_i - v_k||^2 + G_{ki}),$$

and the fuzzy factor is defined as:

$$G_{ki} = \sum_{j\in N_i} \frac{1}{d_{ij}+1}(1 - u_{kj})^{m}||x_j - v_k||^2, \tag{2}$$

where pixel x_i is the central pixel of local window (for example, 3×3), and pixel x_j is in the set of neighbors (N_i) falling into a window around the x_i pixel. d_{ij} is the spatial Euclidean distance between x_i and x_j, and v_k is the prototype of the center of cluster k. With the impact of the fuzzy factor G_{ki}, the noise-corrupted pixels falling into a window retain similar values to the central pixel, and thus FLICM is able to present high robustness to denoise.

2.2 Bias Field and Energy Minimization Formulation

The bias field in a brain MR image can be modeled as a multiplicative component of an observed image[21]. Thus, the observed image can be formulated as:

$$I(x) = b(x)J(x) + n(x), \tag{3}$$

where $I(x)$ is the intensity of original image, $J(x)$ is the true image to be restored, $b(x)$ is an unknown bias field, and $n(x)$ is addictive noise with zero-mean. The aim of the bias field correction is to estimate and eliminate the bias field b. In general, it is assumed that the bias field $b(x)$ varies smoothly in the image region and $J(x)$ is a constant for all pixel x in the k-th tissue[5,7-8].

By seeking the optimal decomposition of image I from (3), the estimation of bias field and tissues segmentation can be formulated as an energy minimization problem. In [1], a novel method which estimates the bias field b and the true image J is proposed. The method considers b and J as the multiplicative intrinsic components of an observed image. Meanwhile, under the prior knowledge about smoothly varying property of the bias field and piecewise constant property of the true image, the energy is minimized in the image domain Ω:

$$F(b, J) = \int_{\Omega} |I(x) - b(x)J(x)|^2 \mathrm{d}x.$$

In theory, an arbitrary function can be approximated by a linear combination of a number of basis functions, while a sufficiently large number M of the

basis functions is given[22]. The bias field can be expressed by a linear combination of a group of smooth basis functions $g_1(x), ..., g_M(x)$[1]. The key problem of having a better expression of bias field is to seek the optimal coefficients $w_1, ..., w_M$ in the linear combination $b(x) = \sum_{k=1}^{M} w_k g_k(x)$. The bias field can be defined as:

$$b(x) = \boldsymbol{w}^{\mathrm{T}} \boldsymbol{G}(x), \tag{4}$$

where the coefficient vector is represented by $\boldsymbol{w} = (w_1, ..., w_M)^{\mathrm{T}}$, and the basis functions are represented by $\boldsymbol{G}(x) = (g_1(x), ..., g_M(x))^{\mathrm{T}}$.

Assumed that the brain MR image has N types of tissues, the gray level of true image $J(x)$ in the i-th cluster is constant c_i approximately. In soft clustering, every pixel has fuzzy membership functions $u_i(x)$ for each cluster center. The fuzzy membership functions can be interpreted as the probability that pixel x belongs to the i-th cluster, and they take values between 0 and 1 following the constraint $\sum_{i=1}^{N} u_i(x) = 1$. Therefore, when the membership functions $u_i(x)$ and cluster center constant c_i are given, the true image can be defined as :

$$J(x) = \sum_{i=1}^{N} c_i u_i(x). \tag{5}$$

Using these definitions of the bias field b and the true image J in (4) and (5) respectively, the objective function $F(b, J)$ can be formulated as[1]:

$$\begin{aligned} F(b, J) &= F(\boldsymbol{u}, \boldsymbol{c}, \boldsymbol{w}) \\ &= \int_{\Omega} |I(x) - \boldsymbol{w}^{\mathrm{T}} \boldsymbol{G}(x) \sum_{i=1}^{N} c_i u_i(x)|^2 \mathrm{d}x, \end{aligned} \tag{6}$$

where $\boldsymbol{G}(x)$ is the basis function, and $\boldsymbol{u} = (u_1, ..., u_N)^{\mathrm{T}}$, $\boldsymbol{c} = (c_1, ..., c_N)^{\mathrm{T}}$ and $\boldsymbol{w} = (w_1, ..., w_N)^{\mathrm{T}}$ are three variables to be determined.

3 Proposed Methods

In this paper, we design a new fuzzy factor, which has a better performance on measuring the influence of the neighborhood pixels. It also takes a full account of the spatial information to reduce the noise sensitivity. Furthermore, we combine the gray-level dissimilarity with membership, and present a new spatial function to improve the efficiency of clustering by updating fuzzy membership. We redefine the objective function by incorporating bias field estimation model to implement bias field estimation and MRI tissues segmentation.

3.1 Improved Fuzzy Factor

The fuzzy factor is aimed at controlling the weight between noise reduction and details reservation. From (2), the fuzzy factor of FLICM algorithm uses only spatial distance factor, which is defined as:

$$\delta_{\mathrm{sd}} = \frac{1}{d_{ij} + 1}. \tag{7}$$

However, it cannot measure the influence between the central pixel and neighbor pixels accurately. For example, as Fig.1 shows below, Fig.1(b) is the gray-level value of a 5×5 local window from original image in Fig.1(a). A, B and C are the neighbor pixels falling into the 3×3 local window of the central pixel, and the local windows of these three pixels are corrupted by noise.

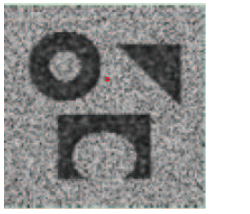

(a)

30	150	30	120	30
30	32	B 52	30	30
100	A 32	30	30	30
30	30	C 30	90	30
30	30	110	30	30

(b)

0.414	B 0.500	0.414
A 0.500	δ_{sd}	0.500
0.414	C 0.500	0.414

(c)

30	32	B 52
100	A 32	30
30	30	C 30

(d)

150	30	120
32	B 52	30
A 32	30	30

(e)

Fig.1. Illustration of (a) original image, (b) gray values of a 5×5 local window, (c) the spatial distance factor of central pixel, (d) the local window of A, and (e) the local window of B.

In (7), A, B and C have the same impact on central pixel (Fig.1(c)). We focus on the local window of A and B. There is a noise pixel in the 3×3 local window of A (Fig.1(d)) while there are two noise pixels in that of B (Fig.1(e)), which implies that the local window of B includes more noise-corrupted pixels. Therefore, A has more impact on central pixel, and thus it should take more weight on the fuzzy factor specifically. For another aspect, there are two noise pixels in the local window of both B and C, but the gray-value difference between B and the central pixel is bigger than that of C. Thus C should take more weight on the fuzzy factor.

The variance coefficient of local window is defined as[23]:

$$C_{\mathrm{u}} = \frac{Var(x)}{(\bar{x})^2},$$

where $Var(x)$ denotes the gray-value variance of local window, and $\bar{x}$ denotes the mean of gray-value. We define the gray-difference coefficient between neighbor pixel x_j and central pixel x_i, as follows:

$$S_{ij} = ||x_j - x_i||, \quad j \in N_i.$$

We normalize the variance coefficient of local window and the gray-difference coefficient to $(0, 1]$ respectively as:

$$\varepsilon_i = \frac{(C_{\mathrm{u}} - C_{\min}) + \xi}{(C_{\max} - C_{\min}) + \xi}, \tag{8}$$

$$\sigma_{ij} = \frac{(S_{ij} - S_{ij(\min)}) + \xi}{(S_{ij(\max)} - S_{ij(\min)}) + \xi}, \quad j \in N_i, \tag{9}$$

where $C_{\min}$ and $C_{\max}$ are the minimum and the maximum of variance coefficients in the local window respectively, and $S_{ij(\min)}$ and $S_{ij(\max)}$ represent the minimum and the maximum of the gray-difference coefficients respectively. The range of values for parameter ξ is (0,1], and this is to ensure ε_i and σ_{ij} unequal to 0. Therefore, the new fuzzy factor δ_{sc} is:

$$\delta_{\mathrm{sc}} = 1 - \log_2 (\sqrt{\varepsilon_j \times \sigma_{ij}} + 1), \quad j \in N_i,$$

where the range of values for the fuzzy factor δ_{sc} is $[0, 1)$. When ε_j and σ_{ij} approach to 1, the local window is corrupted by severe noise or located at the edge of the image, and thus the fuzzy factor is close to 0. On the contrary, when ε_j and σ_{ij} approach to 0, the local window is relatively smooth and the gray-difference is small. The local window is more likely to be partitioned into a same cluster, and thus the fuzzy factor is close to 1. Fig.2 shows the values of ε_j, σ_{ij} and δ_{sc} in the central local window of Fig.1(b), and it clearly illustrates that the new fuzzy factor evaluates the impact of neighbor pixels more completely.

0.837 9	*B* 1.000 0	0.290 4
A 0.155 8	ε_i	0.006 0
0.404 6	*C* 0.332 7	0.337 1

(a)

0.049 2	*B* 0.377 0	0.016 4
A 0.049 2	σ_{ij}	0.016 4
0.016 4	*C* 0.016 4	1.000 0

(b)

0.733 4	*B* 0.309 3	0.903 7
A 0.878 9	δ_{sc}	0.985 8
0.887 0	*C* 0.897 2	0.339 6

(c)

Fig.2. Illustration of the values of (a) variance coefficient ε_i, (b) gray-difference coefficient σ_{ij}, and (c) new fuzzy factor δ_{sc} of the central local window.

From above, we redefine the impact factor which incorporates spatial distance factor δ_{sd} and new fuzzy factor δ_{sc} as follows:

$$\delta_{ij} = \delta_{\mathrm{sd}} \times \delta_{\mathrm{sc}}. \tag{10}$$

The new fuzzy factor considers spatial distance, variance coefficient and gray-difference coefficient simultaneously. Therefore, it is able to achieve better performance on denoising and detail-preserving.

3.2 Spatial Function with Gray-Level Dissimilarity

Considering that these neighbor pixels of an image have similar feature values, the probability that they belong to the same cluster is high[19]. The spatial function represents the probability that pixel i belongs to the k-th cluster, as follows:

$$h_{ik} = \sum_{j \in N_i} \mu_{jk}, \tag{11}$$

where N_i denotes the neighbor pixels around the i-th pixel, and μ_{jk} denotes the membership value of pixel j belonging to the k-th cluster. But (11) only takes the membership values of neighbor pixels into account. As a result, the membership values are almost invariant and the algorithm converges after a lot of iterations. We propose the gray-level dissimilarity $||x_j - x_i||^2$ to overcome the issue mentioned above. Using the new spatial function, our algorithm is able to reduce noise and outliers in the image, and update membership values significantly after each iteration. The new spatial function is defined as follows:

$$f_{ik} = \sum_{j \in N_i} \mu_{jk} \times ||x_j - x_i||^2. \tag{12}$$

We use the following equation to update membership values μ_{ik} for each iteration, where parameters p and q are used to control the relative importance of two functions:

$$\mu'_{ik} = \frac{(\mu_{ik})^p \times (f_{ik})^q}{\sum_{j=1}^{K} (\mu_{ij})^p \times (f_{ij})^q}. \tag{13}$$

There are two cases when the local window is corrupted by noise or outliers. As the 3×3 window shown in Fig.3 and Fig.4, the updated membership values of the non-noisy pixels and the noise-corrupted pixels within a local window are similar to the central pixel, and preserve the insensitiveness to noise.

Case 1. The central pixel is not a noise pixel and some neighbor pixels are corrupted by noise (as shown in Fig.3). It clearly illustrates that the corresponding membership values of the non-noisy pixels and the

noise-corrupted pixels converge to a similar value after three iterations. Generally, the gray-level values of noise-corrupted pixels are far different from those of the other pixels within the window, and thus the new spatial function balances the membership values,

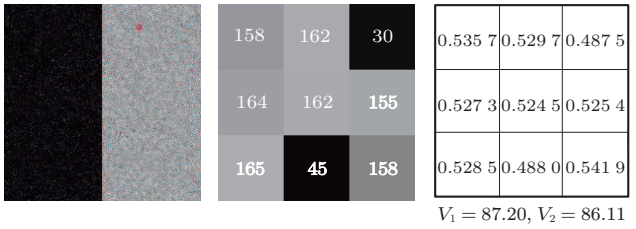

Fig.3. Illustration of the 3×3 window with noise (marked with a square in original image), the cluster center (V_1, V_2) and the corresponding membership values updated by the new spatial function in case 1. (a) Original image. (b) Gray-level values of pixels within the local window. (c) Initial membership values. (d) Membership values after one iteration. (e) Membership values after two iterations. (f) Membership values after three iterations.

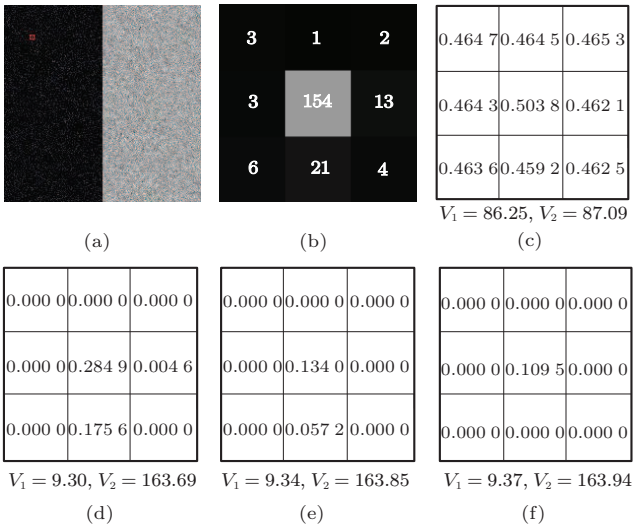

Fig.4. Illustration of the 3×3 window with noise (marked with a square in original image), the cluster center (V_1, V_2) and the corresponding membership values updated by the new spatial function in case 2. (a) Original image. (b) Gray-level values of pixels within the local window. (c) Initial membership values. (d) Membership values after one iteration. (e) Membership values after two iterations. (f) Membership values after three iterations.

and changes their membership values considerably (the updated membership values are equal or close to 1). Therefore, the new spatial function is able to reduce the number of iterations and suppress the influence of noise and outliers.

Case 2. The central pixel is a noise pixel and other pixels are not corrupted by noise (as shown in Fig.4). It clearly shows that the corresponding membership values of neighbor pixels and the central pixel converge to a similar value after three iterations. Similarly, the membership values of these pixels are balanced by the new spatial function, which changes their membership values considerably (the updated membership values are equal or close to 0). Thus, the membership value of the central pixel is not influenced by noise and outliers.

3.3 Objective Function of RCLFCM

In this paper, we propose a new objective function based on the energy minimization formulation (6) and the new fuzzy factor definition (10) as follows:

$$J_{RCLFCM} = \sum_{i=1}^{N}\sum_{k=1}^{c} u_{ki}^{m}||x_i - b_i v_k||^2 + G'_{ki},$$
$$G'_{ki} = \sum_{j \in N_i} \delta_{ij}(1 - u_{kj})^m ||x_j - b_i v_k||^2,$$

where G'_{ki} denotes the new impact factor incorporated with new fuzzy factor δ_{ij}, and x_j denotes the neighbor pixels falling into a window (N_i) around the central pixel x_i. v_k is the prototype of the center of cluster k, and b_i is the intensity of the bias field on pixel x_i.

The energy minimization is performed by minimizing the objective function J_{RCLFCM} alternately with respect to each variable given and the other two fixed. During the whole process, our objective function is constrained by $0 \leqslant u_{ki} \leqslant 1$, $\sum_{k=1}^{K} u_{ki} = 1$. The minimizing of the cluster center v_k and the membership value u_{ki} is obtained as follows:

$$\hat{v_k} = \frac{\sum_{i=1}^{N} b_i \left(u_{ki}^m x_i + \sum_{j \in N_i} \delta_{ij}(1 - u_{kj})^m x_j\right)}{\sum_{i=1}^{N} b_i^2 \left(u_{ki}^m + \sum_{j \in N_i} \delta_{ij}(1 - u_{kj})^m\right)}, \quad (14)$$

$$\hat{u}_{ki} = \frac{1}{\sum_{j=1}^{c} \left(\frac{||x_i - v_k||^2 + G'_{ki}}{||x_i - v_j||^2 + G'_{ji}}\right)^{1/(m-1)}}. \quad (15)$$

We define the intensity of the bias field as the linear combination $b_i = b(i) = \boldsymbol{w}^{\mathrm{T}} \boldsymbol{G}(i)$, where the coefficient is represented by a column vector $\boldsymbol{w} = (w_1, ..., w_M)^{\mathrm{T}}$, and $\boldsymbol{G}(i)$ is the basis function represented by a column

vector $\boldsymbol{G}(i) = (g_1(i), ..., g_M(i))^{\mathrm{T}}$. Minimizing the objective function with respect to coefficient $\boldsymbol{w}$ for fixed v_k and u_{ki} as follows:

$$\hat{\boldsymbol{w}} = \frac{\sum_{i=1}^{N}\sum_{k=1}^{c}\boldsymbol{G}(i)u_{ki}^{m}v_k x_i}{\sum_{i=1}^{N}\sum_{k=1}^{c}\boldsymbol{G}(i)\boldsymbol{G}(i)^{\mathrm{T}}u_{ki}^{m}v_k^2}. \tag{16}$$

With the optimal vector $\hat{\boldsymbol{w}}$ defined in (16), we estimate the bias field computed by:

$$\hat{b}_i = \hat{\boldsymbol{w}}^{\mathrm{T}}\boldsymbol{G}(i). \tag{17}$$

3.4 Implementation

From above, we summarize the RCLFCM algorithm as the iteration processes (as shown in Algorithm 1). The three variables are updated in an iteration process, and each of them is computed with the other two variables. Here, we initialize the cluster center v_k and the membership values u_{ki} in step 1. The convergence criterion used in step 7 is $(\boldsymbol{U}^{(n)} - \boldsymbol{U}^{(n+1)}) \geqslant \varepsilon$, where $\boldsymbol{U}^{(n)}$ is the fuzzy partition matrix $\boldsymbol{U}$ updated in step 6 at the n-th iteration. When the algorithm converges, the maximum membership procedure is used to defuzzify the partition matrix $\boldsymbol{U}$ and assigns pixel i to cluster v_k with the highest membership: $v_k = \arg\{\max\{u_{ki}\}\}, k = 1, 2, ..., c$.

Algorithm 1. *RCLFCM*$(c, m, p, q, \varepsilon)$

Input: the number c of the cluster centers, the weight fuzzy coefficient m, parameters p and q, and the threshold ε

Output: the membership value $\hat{u}_{ki}$, the cluster centers $\hat{v}_k$ and the estimation of the bias field $\hat{b}_i$ when the algorithm converges

1: Initialize the cluster centers v_k and the membership values u_{ki};
2: Set the loop counter $n = 0$;
3: Update b_i as $\hat{b}_i$ in (17);
4: Update v_k as $\hat{v}_k$ in (14);
5: Update u_{ki} as $\hat{u}_{ki}$ in (15);
6: Update $\hat{u}_{ki}$ as $\hat{u}'_{ki}$ in (12) and (13);
7: **if** $(\boldsymbol{U}^{(n)} - \boldsymbol{U}^{(n+1)}) \geqslant \varepsilon$ **then**
8: $n = n + 1$; go to step 3;
9: **else**
10: stop;
11: **end if**

The complexity cost of the bias field update process for each iteration is $O(HW)$, where H and W are the dimensions of the image. The computational complexity of updating both membership matrix and cluster centers is $O(HWc)$ for each iteration, where c is the number of clusters. Therefore, for n iterations, the total computational complexity of the proposed algorithm is $O(nHWc)$.

4 Experimental Results

In this section, we evaluate the performance of proposed RCLFCM algorithm on simulated brain MR images from the BrainWeb① database. This database contains the full simulated brain database and the anatomical model, and provides full three-dimensional data volumes which simulate with three sequences (T1-, T2-, and PD-weighted) and a variety of slice thicknesses, noise levels, and levels of intensity inhomogeneity[24]. We segment the images into GM, WM, CSF and background. Unless otherwise specified, the parameters used in our experiments are set as follows. The number of basis functions is 20. The size of the neighborhood window is 3×3. The weighting exponent m takes its default value 2, and parameters p and q are 2 and 1.5 respectively. Fig.5 shows the average iteration times for different values of parameter ξ in (8) and (9). As we can see from the polyline, when $\xi = 0.1$, the iteration time reaches the minimum. Therefore, we set parameter ξ as 0.1 in the following experiments. All experiments were performed on a PC with an Intel Core-i5 3.20 GHz CPU and 4 GB RAM.

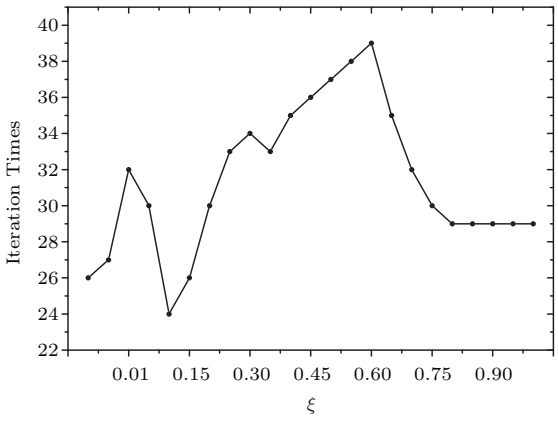

Fig.5. Illustration of the average iteration times for different values of parameter ξ.

Fig.6 illustrates the experimental results of three real brain MR images applying RCLFCM algorithm, including the estimated bias field, images after bias field correction and the tissues segmentation results. The results indicate that the intensity of each tissue becomes

①http://brainweb.bic.mni.mcgill.ca/brainweb/, April 2016.

more uniform after the bias field correction, and we get segmentation results as expected.

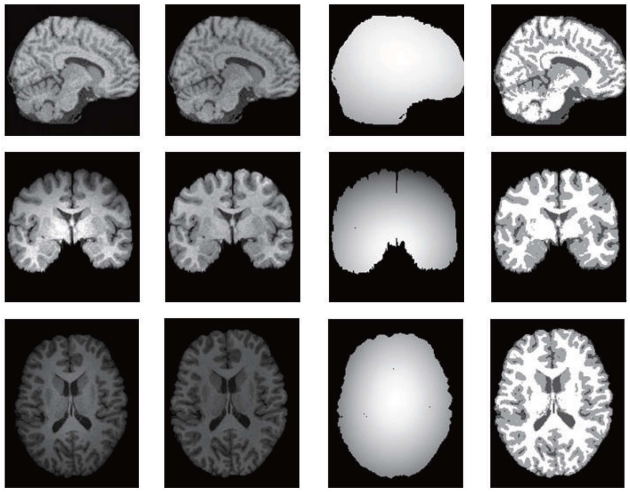

Fig.6. Illustration of the bias field correction and tissues segmentation results by applying RCLFCM algorithm. (a) Three real brain MR images. (b) Images after bias field correction. (c) Estimated bias field. (d) Tissues segmentation results.

We apply the RCLFCM algorithm on synthetic MR brain images, and compare it with five fuzzy algorithms including FCM_S[13], SFCMpq[16], EnFCM[17], FLICM[19] and MICO[1]. Fig.7 shows the ground truth and the clustering results of these methods on T1-weighted, 1 mm synthetic brain MR images with 40% intensity inhomogeneity, which indicates that FCM_S, SFCMCpq and FLICM algorithms are seriously affected by the bias field, and cannot achieve satisfactory results. In contrast, EnFCM, MICO and RCLFCM algorithms get better tissue segmentation results under the intensity inhomogeneity. Among them, RCLFCM retains the original information of images to a large extent.

Furthermore, Fig.8 illustrates the ground truth and the experimental results of the six algorithms on T1-weighted, 1 mm synthetic brain MR images with 40% intensity inhomogeneity and 9% Gaussian noise. Visually, FCM_S, SFCMpq and FLICM algorithms remove most of noise, but they are seriously affected by the bias field. EnFCM and MICO algorithms correct intensity inhomogeneity preferably, but they are sensitive to noise and their results are not satisfactory enough. It clearly shows that the RCLFCM algorithm gives better performance, which segments the tissues of brain accurately and removes almost all noise and outliers.

In order to evaluate the segmentation results quantitatively, this paper uses the segmentation accuracy (SA) to calculate the accuracy of the algorithms. SA is defined as the sum of correctly classified pixels divided by the sum of total number of pixels. The formula is[13]:

$$SA = \sum_{k=1}^{K} \frac{A_k \cap C_k}{\sum_{i=1}^{K} C_i},$$

where K is the number of clusters, A_k denotes the pixels belonging to the k-th cluster for segmentation result,

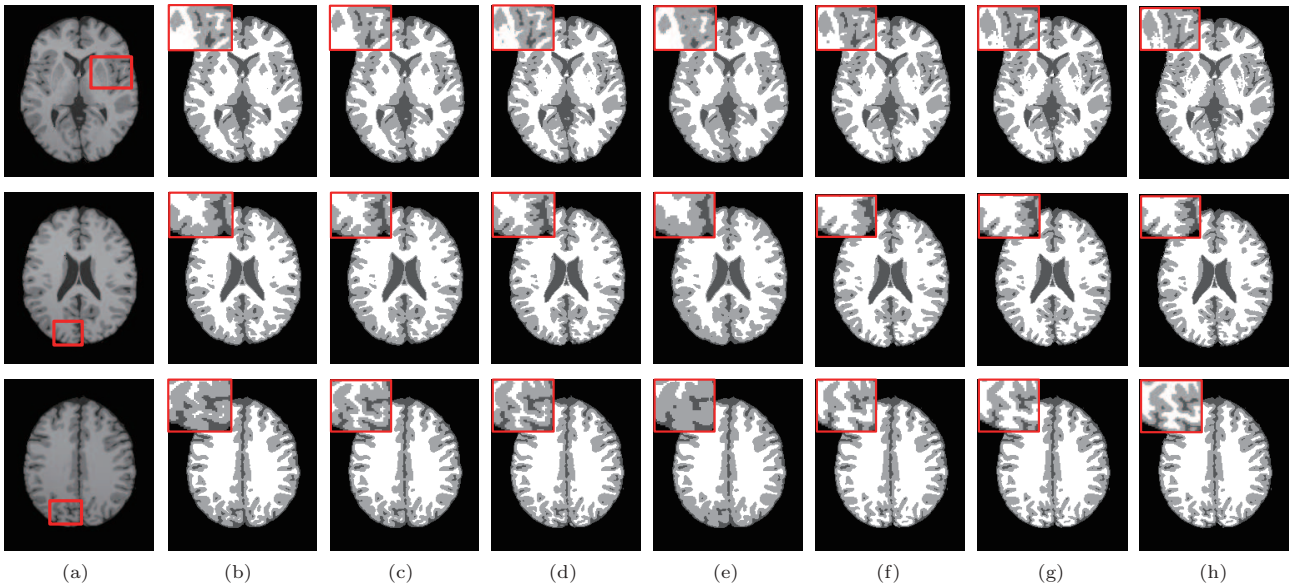

Fig.7. Illustration of (a) three simulated T1-weighted 1 mm brain MR images with 40% intensity inhomogeneity, and segmentation results obtained by applying (b) FCM_S, (c) SFCMpq, (d) EnFCM, (e) FLICM, (f) MICO, and (g) the proposed algorithm RCLFCM. (h) Ground truth.

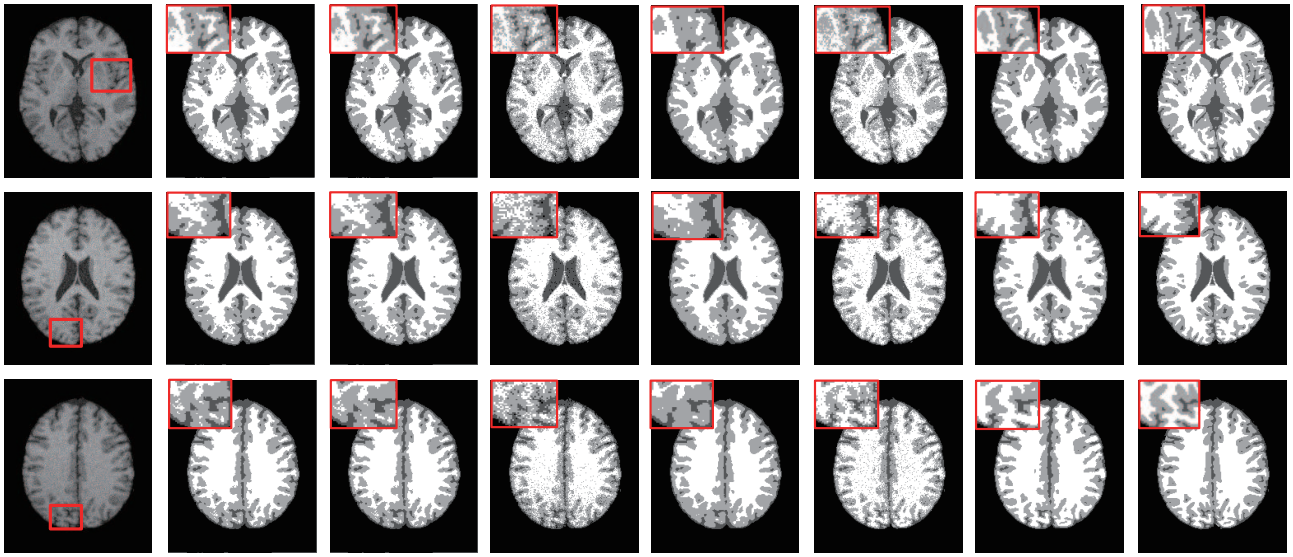

(a) (b) (c) (d) (e) (f) (g) (h)

Fig.8. Illustration of (a) three simulated T1-weighted 1 mm brain MR images with 40% intensity inhomogeneity, and 9% Gaussian noise, and segmentation results obtained by applying (b) FCM_S, (c) SFCMpq, (d) EnFCM, (e) FLICM, (f) MICO, and (g) the proposed algorithm RCLFCM. (h) Ground truth.

and C_k denotes the pixels in the k-th cluster for ground truth.

We evaluate the SA of segmentation results on T1-weighted 1mm synthetic brain MR images with 3%∼9% Gaussian noise and 40% intensity inhomogeneity by applying different algorithms. Table 1 gives the average segmentation accuracy result of the six methods on GM, WM and CSF. From the comparison, it is obvious that the proposed RCLFCM method gives more accurate segmentation result, and retains more details of tissues than the other five methods (the values in bold show higher average segmentation accuracy).

Besides, this paper uses two validity evaluation indexes of clustering V_{pc} and V_{pe} to evaluate algorithms as follows[25]:

$$V_{pc} = \sum_{k=1}^{K}\sum_{i=1}^{N}\frac{u_{ik}^2}{N},$$

$$V_{pe} = -\sum_{k=1}^{K}\sum_{i=1}^{N}\frac{u_{ik}\log(u_{ik})}{N},$$

where u_{ik} is the membership value of pixel i belonging to the k-th cluster, K is the number of clusters and N is the total number of image pixels. When V_{pc} is high and V_{pe} is low, it implies the membership values are less fuzzy in segmentation results and the tissues are classified correctly. We calculate and evaluate the average validity index of the six algorithms. As shown in Fig.9 and Fig.10, it clearly illustrates that RCLFCM has higher V_{pc} and lower V_{pe} compared with other five algorithms, and explains that RCLFCM algorithm is able to achieve more accurate result and less fuzziness in classification.

Table 1. SA Values (Means) of GM, WM and CSF Segmentation

Algorithm	Tissue	Noise (%)			
		3	5	7	9
FCM_S	WM	0.973 4	0.972 6	0.971 0	0.968 2
	GM	0.958 7	0.958 6	0.960 6	0.957 2
	CSF	0.976 1	0.973 9	0.974 0	0.973 4
SFCMpq	WM	0.973 7	0.972 6	0.971 1	0.968 2
	GM	0.959 9	0.958 5	0.956 0	0.951 7
	CSF	0.977 5	0.977 0	0.975 9	0.974 5
EnFCM	WM	0.978 1	0.970 3	0.959 7	0.946 4
	GM	0.969 0	0.959 2	0.945 0	0.924 3
	CSF	0.993 4	0.990 7	0.985 5	0.975 2
FLICM	WM	0.968 9	0.968 1	0.968 1	0.965 9
	GM	0.954 0	0.953 0	0.952 4	0.949 9
	CSF	0.984 2	0.983 9	0.983 6	0.983 2
MICO	WM	0.987 8	0.979 3	0.966 0	0.948 9
	GM	0.979 4	0.969 0	0.952 9	0.932 1
	CSF	**0.994 6**	**0.992 6**	0.989 7	0.985 5
RCLFCM	WM	**0.988 3**	**0.984 5**	**0.977 8**	**0.970 0**
	GM	**0.979 8**	**0.974 1**	**0.966 5**	**0.971 9**
	CSF	0.993 5	0.992 4	**0.991 1**	**0.989 8**

Finally, the average computational cost for each of these six algorithms is illustrated in Fig.11. As shown in the figure below, computational time increases with the increasing of the sizes of images. The quickest

method is EnFCM, while the slowest is FLICM. The proposed method RCLFCM is quite time-consuming, but this drawback is compensated for its better performance as it is shown above. Moreover, our proposed RCLFCM algorithm is easy to implement.

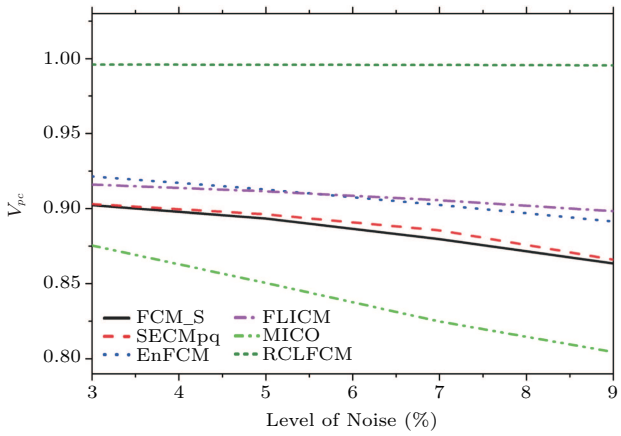

Fig.9. V_{pc} values of segmentation results by applying the six algorithms with increasing noise.

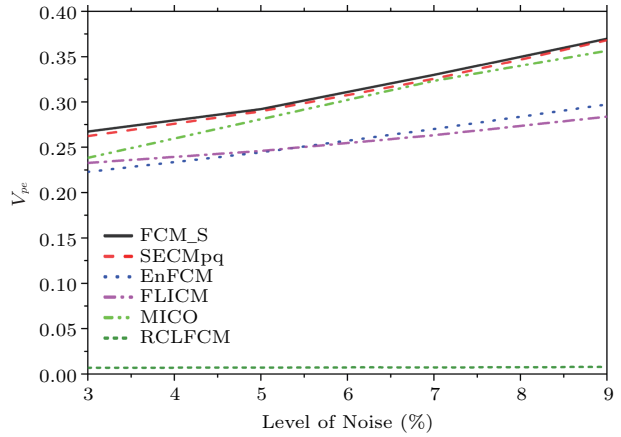

Fig.10. V_{pe} values of segmentation results by applying six algorithms with increasing noise.

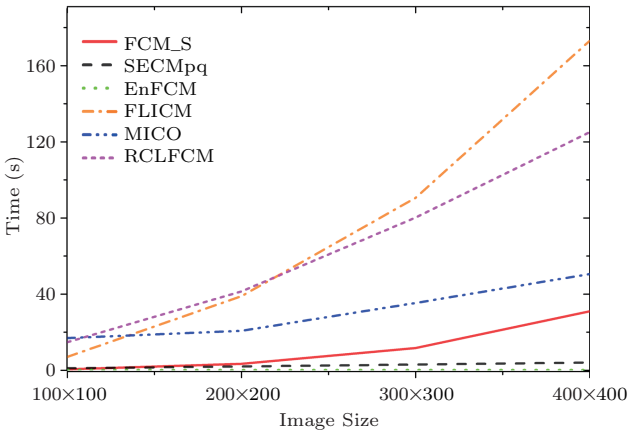

Fig.11. Computational cost (in second) of the six algorithms.

5 Conclusions

In this paper, we proposed a robust algorithm RCLFCM for brain MR image segmentation and bias field correction. In order to take full consideration on neighborhood information and improve the performance of denoising, we designed a gray-different coefficient and defined a new impact factor to measure the effect of the immediate neighborhood. We proposed a new objective function which is based on the bias field model and FCM algorithm. By minimizing the new objective function, we segmented the MR image and corrected the bias field simultaneously, which suppresses the influence of intensity inhomogeneity effectively and achieves better tissues segmentation results. Furthermore, we designed a novel spatial function incorporated with gray-level dissimilarity and membership function, and made full use of the spatial information between pixels to update the membership values in each iteration step, which improves the effectiveness of the clustering algorithm. In the experiment, we applied RCLFCM algorithm on synthetic MR brain images from the BrainWeb database, and compared it with five algorithms. The experimental results showed that the new method can estimate the bias field and suppress the noise effectively, and achieves more accurate segmentation results on brain tissue than the other methods.

References

[1] Li C, Gore J C, Davatzikos C. Multiplicative intrinsic component optimization (MICO) for MRI bias field estimation and tissue segmentation. *Magnetic Resonance Imaging*, 2014, 32(7): 913-923.

[2] Condon B R, Patterson J, Wyper D *et al.* Image nonuniformity in magnetic resonance imaging: Its magnitude and methods for its correction. *The British Journal of Radiology*, 1987, 60(709): 83-87.

[3] Simmons A, Tofts P S, Barker G J *et al.* Sources of intensity nonuniformity in spin echo images at 1.5 T. *Magnetic Resonance in Medicine*, 1994, 32(1): 121-128.

[4] Tincher M, Meyer C R, Gupta R *et al.* Polynomial modeling and reduction of RF body coil spatial inhomogeneity in MRI. *IEEE Transactions on Medical Imaging*, 1993, 12(2): 361-365.

[5] Pham D L, Prince J L. Adaptive fuzzy segmentation of magnetic resonance images. *IEEE Transactions on Medical Imaging*, 1999, 18(9): 737-752.

[6] Styner M, Brechbuhler C, Szckely G *et al.* Parametric estimate of intensity inhomogeneities applied to MRI. *IEEE Transactions on Medical Imaging*, 2000, 19(3): 153-165.

[7] Van Leemput K, Maes F, Vandermeulen D *et al.* Automated model-based bias field correction of MR images of the brain. *IEEE Transactions on Medical Imaging*, 1999, 18(10): 885-896.

[8] Wells III W M, Grimson W E L, Kikinis R *et al*. Adaptive segmentation of MRI data. *IEEE Transactions on Medical Imaging*, 1996, 15(4): 429-442.
[9] Johnston B, Atkins M S, Mackiewich B *et al*. Segmentation of multiple sclerosis lesions in intensity corrected multispectral MRI. *IEEE Transactions on Medical Imaging*, 1996, 15(2): 154-169.
[10] Vovk U, Pernus F, Likar B. A review of methods for correction of intensity inhomogeneity in MRI. *IEEE Transactions on Medical Imaging*, 2007, 26(3): 405-421.
[11] Bezdek J C. Pattern Recognition with Fuzzy Objective Function Algorithms. Springer Science & Business Media, 2013.
[12] Pham D L, Prince J L. An adaptive fuzzy c-means algorithm for image segmentation in the presence of intensity inhomogeneities. *Pattern Recognition Letters*, 1999, 20(1): 57-68.
[13] Ahmed M N, Yamany S M, Mohamed N *et al*. A modified fuzzy c-means algorithm for bias field estimation and segmentation of MRI data. *IEEE Transactions on Medical Imaging*, 2002, 21(3): 193-199.
[14] Balafar M A, Ramli A R, Mashohor S *et al*. Compare different spatial based fuzzy-c-mean (FCM) extensions for MRI image segmentation. In *Proc. the 2nd International Conference on Computer and Automation Engineering* (*ICCAE*), Feb. 2010, pp.609-611.
[15] Chen S, Zhang D. Robust image segmentation using FCM with spatial constraints based on new kernel-induced distance measure. *IEEE Transactions on Systems, Man, and Cybernetics, Part B: Cybernetics*, 2004, 34(4): 1907-1916.
[16] Chuang K S, Tzeng H L, Chen S *et al*. Fuzzy c-means clustering with spatial information for image segmentation. *Computerized Medical Imaging and Graphics*, 2006, 30(1): 9-15.
[17] Szilagyi L, Benyo Z, Szilagyi S M *et al*. MR brain image segmentation using an enhanced fuzzy c-means algorithm. In *Proc. the 25th Annual International Conference of the IEEE Engineering in Medicine and Biology Society*, Sept. 2003, pp.724-726.
[18] Cai W, Chen S, Zhang D. Fast and robust fuzzy c-means clustering algorithms incorporating local information for image segmentation. *Pattern Recognition*, 2007, 40(3): 825-838.
[19] Krinidis S, Chatzis V. A robust fuzzy local information c-means clustering algorithm. *IEEE Transactions on Image Processing*, 2010, 19(5): 1328-1337.
[20] Gong M, Liang Y, Shi J *et al*. Fuzzy c-means clustering with local information and kernel metric for image segmentation. *IEEE Transactions on Image Processing*, 2013, 22(2): 573-584.
[21] Li C, Gatenby C, Wang L *et al*. A robust parametric method for bias field estimation and segmentation of MR images. In *Proc. Computer Vision and Pattern Recognition*, June 2009, pp.218-223.
[22] Powell M J D. Approximation Theory and Methods. Cambridge University Press, 1981.
[23] Gong M, Zhou Z, Ma J. Change detection in synthetic aperture radar images based on image fusion and fuzzy clustering. *IEEE Transactions on Image Processing*, 2012, 21(4): 2141-2151.
[24] Ji Z, Liu J, Cao G *et al*. Robust spatially constrained fuzzy c-means algorithm for brain MR image. *Pattern Recognition*, 2014, 47(7): 2454-2466.
[25] Bezdek J C. Cluster validity with fuzzy sets. *Journal of Cybernetics*, 1973, 3(3): 58-73.

Wen-Qian Deng is currently a M.S. student in the School of Computer Science and Technology, Shandong University, Jinan. She received her B.S. degree in computer science from Shandong University in 2014. Her research interests include medical image processing, computer vision, and CAGD.

Xue-Mei Li received her Master's and Ph.D. degrees in computer science and technology from Shandong University, Jinan, in 2004 and 2010, respectively. She is currently an associate professor in the School of Computer Science and Technology, Shandong University, and a member of the Geometric Design and Information Visualization (GD & IV) Laboratory. She is engaged in research on geometric modeling, CAGD, medical image processing and information visualization.

Xifeng Gao received his M.S. and B.S. degrees, both in computer science from Shandong University, Jinan, in 2011 and 2008, respectively. He is currently a Ph.D. candidate in computer science of the University of Houston. His research interests are computer graphics, geometry processing, medical imaging, and multimedia security.

Cai-Ming Zhang is a professor and doctoral supervisor of the School of Computer Science and Technology at Shandong University, Jinan. He is now also the dean and professor of the Digital Media Research Institute at Shandong University of Finance and Economics, Jinan. He received his B.S. and M.S. degrees in computer science from Shandong University in 1982 and 1984, respectively, and his Ph.D. degree in computer science from the Tokyo Institute of Technology, Japan, in 1994. From 1997 to 2000, Dr. Zhang held visiting position at the University of Kentucky, USA. His research interests include CAGD, CG, information visualization and medical image processing.